JOURNAL OF COMPUTATIONAL PHYSICS 14, 8–28 (1974)

Numerical Method for Predicting Three-Dimensional Steady Viscous Flow in Ducts

W. ROGER BRILEY

United Aircraft Research Laboratories, East Hartford, Connecticut 06108

Received May 7, 1973

A numerical method for predicting three-dimensional, steady viscous flow in ducts is described. The method utilizes approximate governing equations which are applicable to flows having strong convection in one primary flow direction. The governing equations require a coordinate system as input to define primary and secondary flow directions, and an inviscid first approximation to static pressure gradients arising from curved flow geometries. The equations are parabolic and are solved by stepwise integration in the primary flow direction from prescribed upstream initial conditions. Specific details of the method are given by way of application to a special case chosen for its simplicity, that of laminar flow in the entrance region of straight rectangular ducts. A numerical method based on an alternating-direction implicit (ADI) scheme is described and used to compute solutions for flow in ducts having aspect ratios of 1:1 and 2:1; in one case, the effect of thermal convection caused by a transverse buoyancy force is also included. The computed solutions are found to be in good agreement with experimental velocity-profile and pressure-drop measurements. Extensions to treat more general geometries and to include compressibility effects and turbulent transport processes are possible and seem warranted by the present results.

INTRODUCTION

Three-dimensional viscous internal flows occur commonly in practical aerodynamic components. For example, in flows through two-dimensional curved diffusers or through the blade passages of turbomachinery, the turning of the mainstream or primary flow generates a three-dimensional viscous flow in the region of the bounding walls. This flow generally has an important influence on the passage flow losses and, in thermal applications, on the heat transferred to the bounding walls. Small three-dimensional flows occur naturally in the entrance region of straight ducts having nonaxisymmetric cross sections, and much larger secondary flows can be generated in heated or cooled ducts by the presence of transverse buoyancy forces, which result from gravitational, centrifugal, or coriolis accelerations. Obviously, techniques for predicting three-dimensional viscous flows in ducts are of significant practical interest. Because of the interactions which occur

between the inviscid and viscous portions of the flow, the three-dimensional duct flows of interest have been extremely difficult to analyze. Most previous analyses have been based on rotational inviscid flow theory, and much of this effort has been surveyed by Hawthorne [1]. An inviscid "secondary flow approximation" derived by Squire and Winter [2] was applied by them to the flow in a curved rectangular duct, and has been applied recently to the flow in a curved pipe by Rowe [3]. Solutions for both of these problems have been computed recently by Stuart and Hetherington [4] using the full three-dimensional rotational inviscid equations of motion. Although these rotational inviscid analyses are useful and provide considerable insight into the character of three-dimensional duct flows, the neglect of viscous effects is a serious shortcoming if detailed quantitative information is desired. Discrepancies between the inviscid theory and experiment are usually attributed to viscous effects; for example, in the inviscid analysis of flow through a curved duct, the secondary flow produced in the duct depends on the vorticity present in the upstream flow. Since this vorticity normally reaches a maximum in the neglected boundary layer, an arbitrary assumption must be made about where to "cut off" the upstream velocity profile [1], and the resulting solutions are sensitive to the cut-off value (or slip velocity) chosen. Finally, the inviscid theory is not applicable to problems in which the secondary flow is produced entirely within the neglected boundary layers, and cannot be used to compute viscous losses or heat transfer.

In an attempt to account for viscous effects, it is natural to consider using three-dimensional boundary layer theory in conjunction with an inviscid flow analysis. However, such an approach has a number of drawbacks for internal flows. First, the boundary layer equations are not valid in corner regions. Second, the correct means for matching boundary layer and inviscid solutions has not been established if the inviscid flow is rotational. Finally, it is not clear how such an approach could handle strong interaction between viscous and inviscid regions of the type present, for example, in the streamwise "corner vortices" of curved flow passages. An alternate approach is to solve the complete three-dimensional Navier–Stokes equations. Although such an analysis would clearly be adequate to describe the flow in internal flow passages, the grid resolution problems associated with practical high Reynolds number flows, together with the three-dimensionality of the problem, would place excessive demands on the computer time and storage of presently available computers. Although this shortcoming will be mitigated by future generations of computers, the need for a more economical method of analysis remains.

The present method of analysis is an effort to overcome the limitations of the foregoing approaches. The present method utilizes a set of three-dimensional viscous governing equations which are solved by stepwise integration in the direction of the primary flow. The entire flow field is thereby obtained by a sequence of two-

dimensional calculations, and this feature of the method results in a substantial saving of computer time and storage compared to that required for solution of the three-dimensional Navier–Stokes equations. Furthermore, the method adequately treats the corner flow, accounts automatically for interaction between viscous and inviscid flow regions, and is free from the problem of patching boundary layer and inviscid solutions. A similar approach has been taken recently by Patankar and Spalding [5]; their governing equations, except for the transverse buoyancy force, are equivalent to those to be derived here for cartesian coordinates; however, the two methods employ different numerical techniques and differ somewhat in rationale. Another numerical method for the same problem has been proposed by Caretto, Curr, and Spalding [6]. A discussion of the differences between the present method and those of [5] and [6] is postponed to a later section. To gain experience with the present method, and also to develop a sound computational framework which is suitable for extension, the present study was carried out for laminar flow and a simple straight duct geometry. However, the approach taken is reasonably general and can be extended to accommodate flows in curved ducts, turbulent flows, and compressibility.

Formulation of Equations

The governing equations on which the present method is based are derived using what are referred to here as "parabolic flow approximations." The approximations represent an attempt to make use of the experimentally observable fact that high Reynolds number flows in geometries which do not undergo radical changes in the primary flow direction tend to be dominated by upstream conditions rather than by downstream conditions, and that small disturbances at a given point are not transmitted very far upstream of that point. These physical considerations suggest that a reasonable approximation to such a flow can be obtained by a stepwise integration in the direction of the primary flow from a given set of upstream initial conditions, provided a suitable set of governing equations can be found. The parabolic flow approximations require two input items: (1) a coordinate system which defines the primary and secondary flow directions, and (2) a first approximation to the static pressure gradients which arise from curved flow geometries. The coordinate system, which in general would be curvilinear, is shown schematically in Fig. 1. It consists of an axial coordinate which defines the primary flow direction, and two transverse coordinates which define the secondary flow planes. The transverse planes must be perpendicular to the walls, and the walls should, for computational convenience, lie in planes made up of the axial coordinate and one transverse coordinate. The approximation to the static pressure field can be obtained from a potential flow solution for flow through the given geometry, and

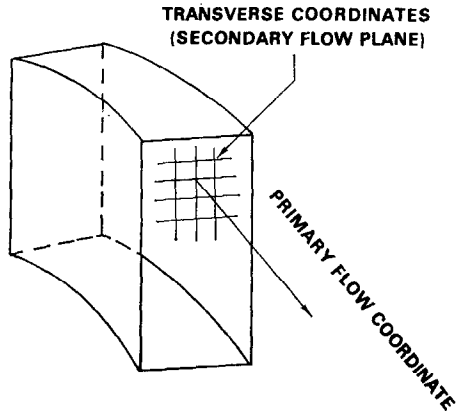

FIG. 1. Schematic of coordinate system for three-dimensional duct flow problem.

is intended to account for the elliptic influence of passage geometry on the flow field. In support of this treatment, it is noted that in many applications not involving primary-flow separation, experimental measurements show that inviscid flow theory yields a good prediction of the static pressure field. Finally, the assumptions are that: (1) viscous diffusion and thermal conduction in the axial or primary flow direction are negligible, and (2) that variations, in the axial and transverse directions, of the viscous correction computed for the pressure field can be treated separately.

Specific details of the present method are presented by way of application to a problem with a simple geometry, that of flow in the entrance region of a straight rectangular duct. A uniform axial velocity with zero secondary flow and constant pressure is assumed at the entrance, and in one calculation, thermal convection caused by a transverse buoyancy force is considered. Since cartesian coordinates are used for this problem, the method is not presented in the full generality contemplated for future applications; however, most of the essential features of the method are present in this simple case. The governing equations are obtained from the steady incompressible Navier–Stokes and energy equations written in cartesian coordinates (x, y, z), with primary flow in the z direction and secondary flow in the x–y plane (see Fig. 2). The Navier–Stokes equations can be written as

$$w\frac{\partial w}{\partial z} = -\frac{1}{\rho}\frac{\partial}{\partial z}(P+p) - u\frac{\partial w}{\partial x} - v\frac{\partial w}{\partial y} + \nu\left[\frac{\partial^2 w}{\partial x^2} + \frac{\partial^2 w}{\partial y^2} + \frac{\partial^2 w}{\partial z^2}\right], \tag{1}$$

$$w\frac{\partial u}{\partial z} = -\frac{1}{\rho}\frac{\partial}{\partial x}(P+p) - u\frac{\partial u}{\partial x} - v\frac{\partial u}{\partial y} + \nu\left[\frac{\partial^2 u}{\partial x^2} + \frac{\partial^2 u}{\partial y^2} + \frac{\partial^2 u}{\partial z^2}\right] + g\beta(T - T_{\text{ref}}), \tag{2}$$

$$w\frac{\partial v}{\partial z} = -\frac{1}{\rho}\frac{\partial}{\partial y}(P+p) - u\frac{\partial v}{\partial x} - v\frac{\partial v}{\partial y} + \nu\left[\frac{\partial^2 v}{\partial x^2} + \frac{\partial^2 v}{\partial y^2} + \frac{\partial^2 v}{\partial z^2}\right], \quad (3)$$

$$w\frac{\partial T}{\partial z} = -u\frac{\partial T}{\partial x} - v\frac{\partial T}{\partial y} + \alpha\left[\frac{\partial^2 T}{\partial x^2} + \frac{\partial^2 T}{\partial y^2} + \frac{\partial^2 T}{\partial z^2}\right], \quad (4)$$

$$\frac{\partial u}{\partial x} + \frac{\partial v}{\partial y} + \frac{\partial w}{\partial z} = 0. \quad (5)$$

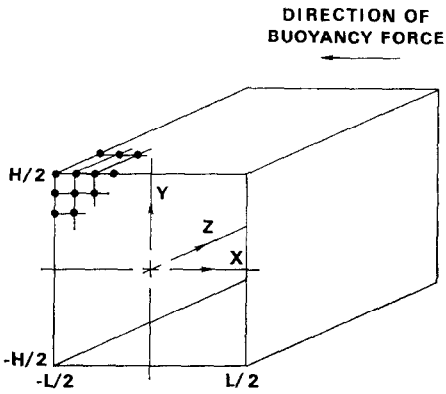

FIG. 2. Coordinate system for straight duct.

In these equations, u, v, and w are velocity components in the x, y, and z directions, respectively; T is temperature; ν is the kinematic viscosity; α is the thermal diffusivity; ρ is the (constant) density, and the static pressure has been written as the sum of an inviscid pressure P, and a viscous pressure correction p, to be explained subsequently. The last term in Eq. (2) is a thermal-convection buoyancy force made up of g, a gravitational or some other acceleration; β, the coefficient of thermal expansion; and $(T - T_{\text{ref}})$, the difference between the local and a reference temperature.

To create a more amenable system of equations, it is assumed that first, streamwise viscous diffusion for all three velocity components, and streamwise thermal conduction can be neglected by dropping the last of the bracketed terms in each of Eqs. (1)–(4) (i.e., all second derivatives with respect to the primary flow or z direction are discarded). Second, the inviscid pressure P, is assumed to be known from a potential flow solution and the components of its gradient are treated as source terms. For the straight duct problem, the potential flow with constant axial velocity and pressure is used, and in this special case, P is constant and its gradient is zero. Finally, as originally suggested by Patankar and Spalding [5], the viscous pressure correction p, in the primary flow equation (1), is treated separately from that in the secondary flow equations (2) and (3). In Eq. (1), the $\partial p/\partial z$ term is

redefined to be a mean viscous pressure drop which is a function of z only (i.e., constant in the x–y plane) and is computed as part of the solution from the requirement that the integral mass flow in the axial direction be conserved. Thus, $\partial p/\partial z$ is replaced by $dp_m(z)/dz$. No restrictions are placed on p in the secondary flow equations; in effect, p is required to vary in the x–y plane in such a way as to ensure that the continuity equation (5), is satisfied at every point in the flow field. With these assumptions, the governing equations for the straight duct become

$$w\frac{\partial w}{\partial z} = -\frac{1}{\rho}\frac{d}{dz}p_m(z) - u\frac{\partial w}{\partial x} - v\frac{\partial w}{\partial y} + \nu\left[\frac{\partial^2 w}{\partial x^2} + \frac{\partial^2 w}{\partial y^2}\right], \tag{6}$$

$$w\frac{\partial u}{\partial z} = -\frac{1}{\rho}\frac{\partial p}{\partial x} - u\frac{\partial u}{\partial x} - v\frac{\partial u}{\partial y} + \nu\left[\frac{\partial^2 u}{\partial x^2} + \frac{\partial^2 u}{\partial y^2}\right] + g\beta(T - T_{\text{ref}}), \tag{7}$$

$$w\frac{\partial v}{\partial z} = -\frac{1}{\rho}\frac{\partial p}{\partial y} - u\frac{\partial v}{\partial x} - v\frac{\partial v}{\partial y} + \nu\left[\frac{\partial^2 v}{\partial x^2} + \frac{\partial^2 v}{\partial y^2}\right], \tag{8}$$

$$w\frac{\partial T}{\partial z} = -u\frac{\partial T}{\partial x} - v\frac{\partial T}{\partial y} + \alpha\left[\frac{\partial^2 T}{\partial x^2} + \frac{\partial^2 T}{\partial y^2}\right], \tag{9}$$

$$\frac{\partial u}{\partial x} + \frac{\partial v}{\partial y} + \frac{\partial w}{\partial z} = 0, \tag{10}$$

together with the integral constraint on mass flow through the duct, which for impermeable walls can be written as

$$\int_{-H/2}^{H/2}\int_{-L/2}^{L/2} w\,dx\,dy = \frac{\dot{m}}{\rho}, \tag{11}$$

where $\dot{m}$ is the mass flow rate through the duct. It can be shown that the set of equations (6)–(11) constitute a parabolic system and can be solved by stepwise integration in the axial or z direction from a specified set of upstream initial conditions. The problem formulation is completed by specifying boundary and initial conditions. It is assumed that the fluid entering the duct has a uniform axial velocity with no secondary flow, and constant pressure and temperature. No-slip conditions are specified on the duct walls. Solutions are computed for two problems: (1) pure hydrodynamic flow development (i.e., isothermal flow), and (2) the mixed convection problem in which the wall temperature is uniform at each axial location, but increases linearly with axial distance.

As partial justification for the parabolic flow approximations, it is noted that since the coordinate system is chosen so that the transverse x–y planes are perpendicular to the duct walls, the analysis takes full account of viscous diffusion normal to the walls, which is known to be important from considerations of boundary layer theory. The treatment of pressure terms is based in part on the experience

that potential flow analysis yields a good prediction of the pressure field in many cases of interest. The inviscid pressure P, accounts a priori for the elliptic influence of a curved geometry, in much the same way that a pressure distribution is "imposed" in boundary layer solutions. The separate treatment given to viscous pressure correction terms in the primary and secondary flow equations is necessary to obtain a parabolic set of equations. The assumption that p_m is constant in transverse planes is reasonable for flow in a straight duct, except where inlet conditions imply a singularity, but this particular assumption for p_m is not essential.

One important restriction arises from the parabolic character of the governing equations: the axial or primary flow velocity component must remain positive. In other words, there can be no separation of the primary flow; secondary flow separation can occur, however, and thus the equations possess the necessary generality to describe the formation of streamwise vortices. Clearly, however, the analysis is not intended for application to geometries having abrupt changes in cross sectional area or to flow through sharp elbows, since the primary flow separates in these cases. The application to flow in a straight rectangular duct provides a test of all of the essential features of the method except the important one in which a nontrivial estimate for the inviscid static pressure field P, is required, as would be the case if the duct were curved; however, such extensions are reserved for a future study.

The Numerical Method

In this section, a finite-difference procedure for solving Eqs. (6)–(11), based on an alternating-direction implicit (ADI) method, is described. As mentioned earlier, numerical methods for essentially the same equations have been proposed in [5] and [6]. The method of Caretto, Curr, and Spalding [6] is implicit and involves the simultaneous solution of coupled nonlinear difference equations, thereby avoiding the need for linearizing and decoupling assumptions. The solution procedure, however, is a point-by-point iteration method which may be expected to have slow convergence properties, particularly for cases with small grid spacing. In the method of Patankar and Spalding [5], the equations are linearized and decoupled, and in the computation of secondary flow, corrections for predicted secondary flow velocities and pressure are calculated simultaneously by iteratively solving a single Poisson-like equation for the pressure correction. The simultaneous solution of velocity and pressure corrections was made possible by neglecting off-diagonal velocity terms in the difference equations for velocity corrections. In the method proposed here, these terms are retained as it appears they are negligible only for sufficiently small axial step size, and the assumption is instead made that the velocity corrections are irrotational. Although the present method thereby requires

the solution of two Poisson equations, one for a potential for the velocity correction and one for the pressure field, it is believed that greater accuracy will result for a given choice of grid spacing and axial step size.

Background for the Solution Procedure

To implement the procedure, the flow region is discretized by grid points having equal spacings Δx and Δy, in the x and y directions, respectively, and an arbitrary axial step size Δz. The subscripts i and j, and the superscript n, are grid point indices associated with x, y, and z, respectively. Thus, $\phi^n_{i,j}$ denotes $\phi(x_i, y_j, z^n)$, where ϕ is a dummy symbol representing any one of the dependent variables. The subscripts are frequently omitted, so that ϕ^n is equivalent to $\phi^n_{i,j}$. For convenience, the following shorthand difference-operator notation is used for derivative difference formulas:

$$\delta_x \phi^n_{i,j} = \frac{\phi^n_{i+1,j} - \phi^n_{i-1,j}}{2\Delta x} = \frac{\partial \phi}{\partial x}\bigg|^n_{i,j} + O(\Delta x)^2, \tag{12}$$

$$\delta_x{}^2 \phi^n_{i,j} = \frac{\phi^n_{i+1,j} - 2\phi^n_{i,j} + \phi^n_{i+1,j}}{(\Delta x)^2} = \frac{\partial^2 \phi}{\partial x^2}\bigg|^n_{i,j} + O(\Delta x)^2, \tag{13}$$

with corresponding definitions for $\delta_y \phi^n_{i,j}$ and $\delta_y{}^2 \phi^n_{i,j}$. It is assumed that the solution is known at the n level, z^n, and that values for u^{n+1}, v^{n+1}, w^{n+1}, p^{n+1}, and T^{n+1} are to be computed. In general terms, the procedure is as follows.

(1) w^{n+1} is computed from the axial momentum equation, Eq. (6), with p^{n+1}_m determined implicitly to ensure that the axial mass flow relation (11), is satisfied.

(2) First approximations to u^{n+1} and v^{n+1} are computed from the transverse momentum equations (7) and (8). Small corrections are computed from the requirement that u^{n+1} and v^{n+1} satisfy continuity, Eq. (10), in a manner to be explained subsequently.

(3) p^{n+1} is computed from a Poisson equation for pressure constructed from the transverse momentum equations (7) and (8), which are evaluated using the corrected values for u^{n+1} and v^{n+1}.

(4) T^{n+1} is computed from the energy equation (9).

To carry out the foregoing procedure, it is noted that each of Eqs. (6)–(8) can be written in the form

$$w \frac{\partial \phi}{\partial z} = L^2 \phi + S_\phi \tag{14}$$

where ϕ denotes any of the dependent variables u, v, or w; L^2 is a second-order differential operator such that

$$L^2 = -u\frac{\partial}{\partial x} - v\frac{\partial}{\partial y} + \nu\left[\frac{\partial^2}{\partial x^2} + \frac{\partial^2}{\partial y^2}\right] \tag{15}$$

and S_ϕ is treated as a source term which includes appropriate pressure gradient and/or buoyancy force terms. If ν is replaced by α in Eq. (15), then Eq. (9) also has the form of Eq. (14). To solve any one of the equations represented by Eq. (14), the coefficients w, u, and v, and source term S_ϕ in Eqs. (14) and (15) are lagged (i.e., evaluated from known values at the n level) and the resulting equations are differenced using a Crank–Nicolson-type replacement of spatial derivatives. Thus, Eqs. (14) and (15) become

$$w^n\frac{\phi^{n+1} - \phi^n}{\Delta z} = D^2\left[\frac{\phi^{n+1} + \phi^n}{2}\right] + (S_\phi)^n \tag{16}$$

where D^2 is the following linearized second-order difference operator.

$$D^2 = -u^n\delta_x - v^n\delta_y + \nu[\delta_x{}^2 + \delta_y{}^2]. \tag{17}$$

This treatment constitutes a numerical linearization and decoupling of Eqs. (6)–(9). It is understood that the D^2 operator in Eq. (17) can be split into separate terms and applied to ϕ evaluated at the n, $(n + 1)$, or intermediate levels as required by the ADI method to be described. To solve the equations represented by Eq. (16), ADI techniques which are unconditionally stable (in the usual linearized sense) are preferred to explicit methods which suffer from one or more stability restrictions and which, therefore, require an axial step size Δz, limited by the grid spacing rather than by the rate at which physical variables are changing with axial distance. The technique of Douglas and Gunn [7] was used here to generate an ADI scheme from the basic Crank–Nicolson scheme of Eq. (16). As with other ADI schemes, the Douglas–Gunn scheme computes the solution for an axial step in two steps, each of which involves treating derivatives implicitly in one of the coordinate directions. The difference equations for the two steps are

$$w^n\left(\frac{\phi^* - \phi^n}{\Delta z}\right) = [-u^n\delta_x + \nu\delta_x{}^2]\left(\frac{\phi^* + \phi^n}{2}\right) + [-v^n\delta_y + \nu\delta_y{}^2](\phi^n) + (S_\phi)^n, \tag{18a}$$

$$w^n\left(\frac{\phi^{**} - \phi^n}{\Delta z}\right) = [-u^n\delta_x + \nu\delta_x{}^2]\left(\frac{\phi^* + \phi^n}{2}\right) + [-v^n\delta_y + \nu\delta_y{}^2]\left(\frac{\phi^{**} + \phi^n}{2}\right) + (S_\phi)^n. \tag{18b}$$

During the first step of the ADI procedure, Eq. (18a) is applied at successive x-direction rows of grid points to provide systems of algebraic equations which are linear in the implicit intermediate quantity ϕ^* and which have a tridiagonal matrix structure. These tridiagonal systems can be solved by any one of several efficient algorithms; the method used here is a straightforward modification of Gaussian elimination in which the nontridiagonal matrix elements (which are zero) are ignored. The second step of the ADI procedure is similar to the first except that Eq. (18b) is applied along successive y-direction rows of grid points to obtain implicit equations for ϕ^{**}. As shown by Douglas and Gunn [7], the final solution, ϕ^{**} approximates ϕ^{n+1} to the same order of accuracy as the truncation error in Eq. (16); consequently, ϕ^{**} is accepted as ϕ^{n+1}. For programming purposes, Eq. (18b) can be simplified by subtracting Eq. (18a) from Eq. (18b). Having established the necessary background information, specific details of the procedure for advancing the solution from the n to the $(n + 1)$ level are now discussed.

Computation of Axial Velocity and Pressure Drop

The first step of the present method is to compute w^{n+1} from Eq. (6). The mean pressure drop term in Eq. (6) is differenced as follows.

$$(d/dz)\, p_m(z) = (p_m^{n+1} - p_m{}^n)/\Delta z \tag{19}$$

and treated as a source term. Since p_m^{n+1} is initially unknown, the correct value of p_m^{n+1} is obtained implicitly using the standard secant iteration technique [8]. The procedure is to assume a value for p_m^{n+1}, solve the axial momentum equation (6), for the w^{n+1} field using the ADI technique defined by Eqs. (18), compute the axial mass flow rate from w^{n+1} by two-dimensional numerical integration, and repeat this process using the secant method to find the value of p_m^{n+1} which leads to a w^{n+1} which satisfies the integral mass flow constraint, Eq. (11). Because of the linear character of the difference equations, the secant method converges to the limit of machine accuracy in three iterations. The boundary conditions for w^{n+1} are that w^{n+1} is zero at points on the wall.

Computation of Remaining Variables

The next step of the method is to compute values for u^{n+1}, v^{n+1}, and p^{n+1} which satisfy the transverse momentum equations (7) and (8), and the continuity equation (10). To this end, the following decomposition of u^{n+1} and v^{n+1} is performed:

$$u^{n+1} = u_p + u_c\,, \qquad v^{n+1} = v_p + v_c\,, \tag{20}$$

where u_p and v_p are *predictions* of u^{n+1} and v^{n+1} computed from the secondary flow momentum equations, and u_c and v_c are $O(\Delta z)$ *corrections* to u_p and v_p which ensure that u^{n+1} and v^{n+1} satisfy the continuity equation. The velocity predictions and

corrections are defined by the procedures used to calculate them, as follows. The velocity predictions u_p and v_p, are simply the approximations to u^{n+1} and v^{n+1} which result from straightforward solution of the transverse momentum equations (7) and (8), using the ADI technique defined by Eqs. (18). For example, if ϕ in Eqs. (18) represents u, then the solution of Eqs. (18) will be u^{**}, which is by definition u_p. The boundary conditions are that u_p and v_p vanish at the walls. Values of p^{n+1} are not required to compute u_p and v_p since the pressure gradient terms in Eqs. (16) and (17) are evaluated at the n level. The corrections, u_c and v_c, are of order Δz and are computed from the requirement that u^{n+1} and v^{n+1} satisfy a difference form of the continuity equation. Combining Eqs. (10) and (20),

$$\frac{\partial u^{n+1}}{\partial x} + \frac{\partial v^{n+1}}{\partial y} = \left(\frac{\partial u_p}{\partial x} + \frac{\partial v_p}{\partial y}\right) + \left(\frac{\partial u_c}{\partial x} + \frac{\partial v_c}{\partial y}\right) = -\frac{\partial w}{\partial z}. \tag{21}$$

It is assumed that the velocity corrections are irrotational, and a velocity potential Φ, is introduced such that

$$u_c = \partial\Phi/\partial x, \qquad v_c = \partial\Phi/\partial y. \tag{22}$$

The solenoidal contribution to the velocity corrections is of order Δz and does not affect the continuity equation; since the momentum equations are already satisfied to $O(\Delta z)$, this contribution is neglected. Equation (22) is combined with Eq. (21) and the result differenced to obtain

$$(\delta_x{}^2 + \delta_y{}^2)\,\Phi = -\left[\delta_x(u_p) + \delta_y(v_p) + \frac{(w^{n+1} - w^n)}{\Delta z}\right]. \tag{23}$$

Equation (23) is a difference form of Poisson's equation, and since all quantities on the right-hand side of this equation are known, it can be solved by any of the standard methods for Poisson's equation. The method of successive over-relaxation (SOR) by points was used here. It is noted, however, that SOR was considered adequate in the present case only because the solutions did not require much computer time; a more efficient technique such as ADI, block over-relaxation, or a fast direct method is recommended for cases in which computer time is of greater concern. Boundary conditions for Eq. (23) are that the velocity component (u_c or v_c) normal to the walls is zero, and hence the normal derivatives of Φ vanish. Since u_p and v_p are not known at points outside the walls, it is necessary to evaluate the normal derivatives of u_p and v_p at the walls, when required in Eq. (23), using three-point, one-sided, second-order accurate difference formulas. Once Φ has been computed, u_c and v_c are known by definition, and u^{n+1} and v^{n+1} are computed from Eq. (20). It is noted that u_c, v_c, and hence, u^{n+1}, v^{n+1} will not in general satisfy the no-slip conditions exactly, since only one velocity component can be specified as

boundary conditions for Eq. (23). However, the no-slip conditions are satisfied to $O(\Delta z)$ since u_c and v_c are $O(\Delta z)$ corrections added to u_p and v_p, which in turn satisfy the no-slip conditions. The small slip values for u^{n+1} and v^{n+1} could, of course, be reset to zero if desired; however, this was not done in the present solutions. In either case, the magnitude of the slip values provides a convenient test of the axial resolution of the method; if the boundary slip velocities are not negligible when compared with secondary flow velocities in the interior, the axial step size should be reduced accordingly. Once u^{n+1} and v^{n+1} have been computed, advanced values for pressure p^{n+1}, are computed from the secondary flow momentum equations. To accomplish this, the differenced forms of Eqs. (7–8) are evaluated using u^{n+1} and v^{n+1} to obtain components of the gradient of p^{n+1} as follows.

$$\left(\frac{\partial p}{\partial x}\right)_{i,j}^{n+1} = (F_1)_{i,j} = \rho\left[-w^n \frac{(u^{n+1} - u^n)}{\Delta z} + D^2 u^{n+1} + g\beta(T - T_{\text{ref}})\right], \quad (24)$$

$$\left(\frac{\partial p}{\partial y}\right)_{i,j}^{n+1} = (F_2)_{i,j} = \rho\left[-w^n \frac{(v^{n+1} - v^n)}{\Delta z} + D^2 v^{n+1}\right], \quad (25)$$

where F_1 and F_2 are introduced for notational convenience. To construct p^{n+1}, a Poisson equation for p^{n+1} is formed by differentiating and adding Eqs. (24) and (25) as follows.

$$\left[\frac{\partial^2 p}{\partial x^2} + \frac{\partial^2 p}{\partial y^2}\right]_{i,j}^{n+1} = \left[\frac{\partial F_1}{\partial x} + \frac{\partial F_2}{\partial y}\right]_{i,j}, \quad (26)$$

and expressing this equation in difference form as

$$(\delta_x^2 + \delta_y^2)\, p^{n+1} = \delta_x(F_1) + \delta_y(F_2). \quad (27)$$

Equation (27) has the same form as Eq. (23) and was also solved using SOR. The quantities F_1 and F_2 can be evaluated from Eqs. (24) and (25) everywhere except on the walls; therefore, Eq. (27) is solved in the region bounded by the rows of grid points immediately adjacent to the walls, and boundary conditions are applied at these grid points. The normal derivatives of p^{n+1} on this computational boundary are known from Eqs. (24) and (25), and these are used as boundary conditions. With this treatment, p^{n+1} is determined at every point in the cross-sectional plane, including points on the walls. The derivatives of F_1 and F_2 appearing in the source term of Eq. (27) are computed with central difference formulas, as indicated by Eq. (27), except at the points immediately adjacent to the walls, where these formulas would require unknown values of F_1 and F_2 on the walls. At these points, three-point, one-sided difference formulas are used.

The final step in the method is to compute values for T^{n+1}; this is accomplished without difficulty by application of the ADI technique defined by Eqs. (18) to the temperature equation (9).

Further Computational Details

In the solution of Eq. (23) for Φ and Eq. (27) for p^{n+1}, consideration must be given to an integral constraint which arises when solving the Poisson equation with normal derivative boundary conditions. The constraint is well known and is a consequence of the fact that a solution to the two-dimensional Poisson equation for ϕ with source distribution $f(x, y)$, and Neumann boundary conditions exists only if the following condition is satisfied:

$$\int_A f(x, y)\, dA = \int_C \frac{\partial \phi}{\partial n}\, ds, \tag{28}$$

where A is the area enclosed by C, the boundary of the solution domain; n is the outward normal to C, and s is distance along C. Equation (28) is a consequence of Green's first integral theorem [9]. Because of truncation error, the right-hand sides of Eqs. (23) and (27) will not, in general, satisfy this integral constraint exactly. To correct for this inconsistency, a small uniform correction was added to the Poisson source distribution. To compute the required correction, the quantity, E, defined by

$$E = \int_A f(x, y)\, dA - \int_C \frac{\partial \phi}{\partial n}\, ds \tag{29}$$

was computed by numerical integration before solving Eq. (23) or Eq. (27). The area-averaged amount by which the right-hand sides of Eq. (23) or Eq. (27) fail to satisfy the finite-difference analog of Eq. (28) is then given by $(\Delta f)_{\text{ave}} = E/A$. This constant amount $(\Delta f)_{\text{ave}}$, is therefore subtracted from the right-hand sides of Eqs. (23) or (27) at each grid point, to comply with the integral constraint. With this correction properly taken into account, solutions to Eqs. (23) and (27) exist and are unique to within an arbitrary constant. Failure to comply with the integral constraint causes a slow divergence of the SOR iteration.

It remains to specify the treatment of initial conditions, a delicate matter for the present problem, since the initial conditions are singular. The singularity is a result of the assumption that the axial velocity is impulsively reduced from its inlet value to zero on the walls at the duct entrance. This mathematical treatment implies that the boundary layers initially have zero thickness and infinite transverse velocity and pressure gradients. Obviously, the present difference method with its finite mesh spacing cannot handle these conditions without large errors near the singularity. However, from a computational standpoint, it is characteristic of parabolic equations for the initial error to decay rather quickly as integration proceeds away from the singularity into a region where the mesh spacing provides sufficient resolution [10]; therefore, it is believed that the solutions presented are accurate except near the duct entrance. This conclusion was reinforced by numerical experiments in which different grid spacings and axial step sizes were used. For a

typical solution, decreasing the mesh spacing by 50% and varying the step size up to 100% had no appreciable effect on the solution except very near the duct entrance. Further consideration will be given to starting error in the discussion of results. Numerically, the treatment of the first axial step is the same as subsequent steps, except that the computation of the transverse pressure p, is omitted to avoid generating "impulsive" pressure due to the sudden appearance of secondary flow.

Computed Results and Comparison with Experiment

In this section, solutions are presented for two ducts having aspect ratios H/L, of 1 : 1 and 2 : 1. These solutions are presented in nondimensional form and are compared with experimental velocity profile and pressure drop measurements from three sources [11–13]. The following definitions are applicable. D is the hydraulic diameter, equal to four times the cross-sectional area of the duct divided by its perimeter; w_0 and p_0 are the axial velocity and static pressure at the duct entrance; w_{CL} is the centerline axial velocity; and Re is the Reynolds number $w_0 D/\nu$. The solutions were computed for Reynolds numbers of 1000 and 1333, respectively, for the 1:1 and 2:1 ducts.

The computed mean pressure drop and centerline velocity development are shown in Figs. 3 and 4 for the two ducts, and these are found to be in good agreement with the experiment measurements. The effect on centerline velocity development of neglecting the secondary flow is shown in Fig. 4. The secondary flow has only a mild influence on the primary flow because the transverse velocity components are relatively small. The magnitude of u and v varies with Reynolds number, but for these solutions u and v were of the order of a few tenths of one percent of w_0. A more detailed comparison with experiment of the axial velocity development is given in Figs. 5 and 6, where velocity profiles at selected axial locations are shown; again the computed and experimental results are in good agreement. Computed secondary-flow velocity profiles at one axial location are shown in Figs. 7 and 8 for each of the two ducts. The secondary flow is away from the walls and toward the center of the duct, and supplies fluid to the accelerating axial flow in the central core of the duct. It is perhaps worth noting that the secondary flow does not have a structure consisting of streamwise vortices.

The error in these solutions caused by singular starting conditions can be examined to a limited extent by means of a simple analysis. Citing the analysis of Schlichting [14] for a two-dimensional channel, Sparrow *et al.* [12] have pointed out that near the duct entrance, w_{CL} should vary in accordance with

$$w_{CL}/w_0 = 1 + cz^{1/2} + \cdots, \tag{30}$$

where c is a constant of proportionality. Thus, near the duct entrance, a plot of

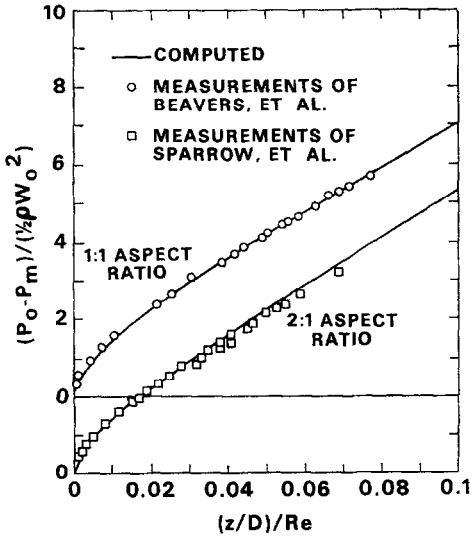

FIG. 3. Pressure drop coefficient, $(p_0 - p_m)/((1/2)\rho w_0^2)$, vs nondimensional axial distance, (z/D)/Re, for rectangular ducts.

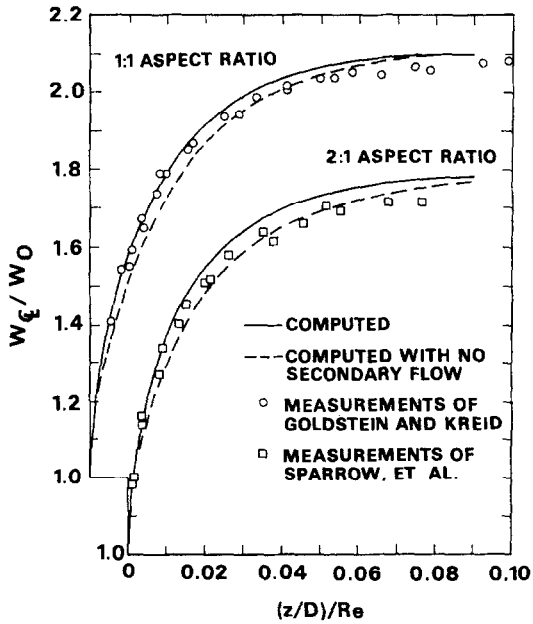

FIG. 4. Centerline velocity ratio, w_{CL}/w_0, vs nondimensional axial distance, (z/D)/Re, for rectangular ducts.

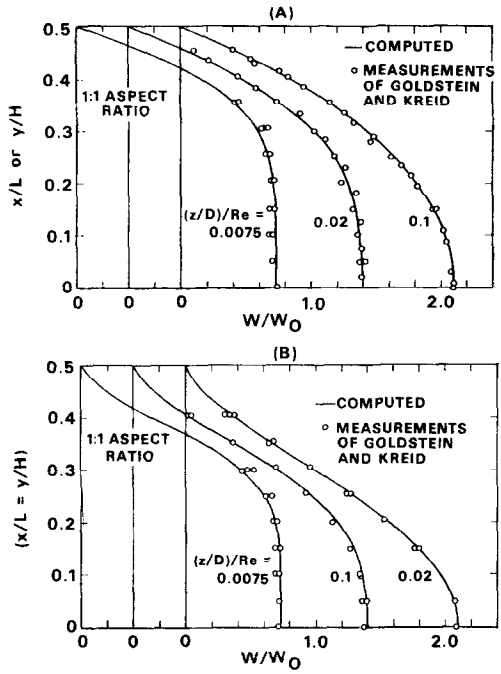

FIG. 5. Nondimensional transverse distance vs axial velocity ratio w/w_0, at selected axial locations for a square duct; (A) profiles at $x/L = 0$ or $y/H = 0$; (B) profiles along a diagonal.

w_{CL} versus $z^{1/2}$ should have a constant slope, $dw_{CL}/d(z^{1/2})$. In Fig. 9, both of these quantities are plotted in nondimensional form for the square duct solution, and an irregular behavior during the first twelve or so axial steps is evident, particularly in the computed values of slope. An extrapolated curve for slope, which has starting behavior of the type suggested by Eq. (30), is also shown, and this curve suggests that the slope should have a value of approximately 6 at the origin. By fitting a straight line with a slope of 6 to the computed points for velocity, as shown in Fig. 9, a virtual origin for the solution can be found; in this case, the virtual origin is located at $Z = -0.05$, where Z is the nondimensional axial variable, $[(z/D)/\mathrm{Re}]^{1/2}$. Using this procedure, a small correction for starting error was made to each solution by redefining the Z axis (using a simple translation of the origin) to make the actual and virtual origins coincide.

As mentioned previously, the secondary flow is relatively small for the isothermal solutions in Figs. 3–8. To demonstrate the applicability of the method to a case with larger secondary flow, a solution was computed for a flow with mixed convection caused by a transverse buoyancy force. In this solution, the wall temperature T_w, is constant at each axial location and increases linearly in the z direction. The

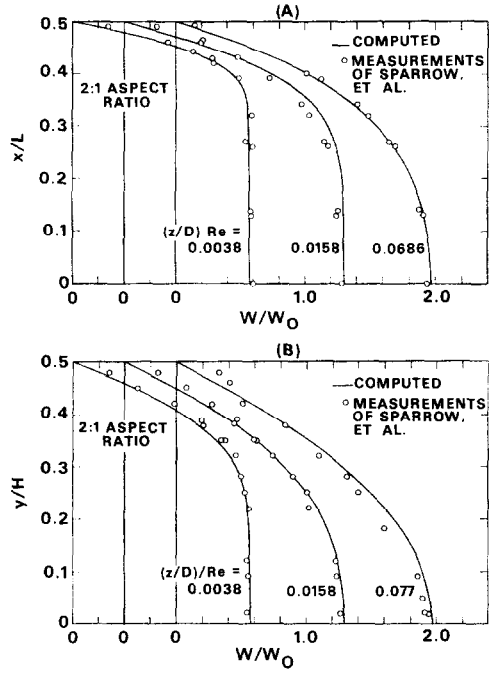

FIG. 6. Nondimensional transverse distance vs axial velocity ratio w/w_0, at selected axial locations for a duct with 2:1 aspect ratio: (A) profiles across wide dimension, $y/H = 0$; (B) profiles across narrow dimension, $x/L = 0$.

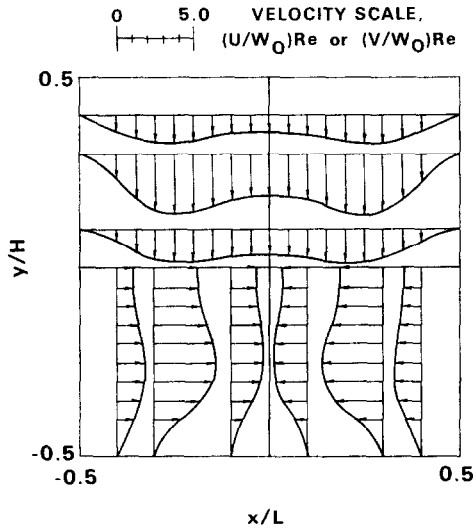

FIG. 7. Secondary flow velocity profiles for a square duct, $(z/D)/\mathrm{Re} = 0.0075$.

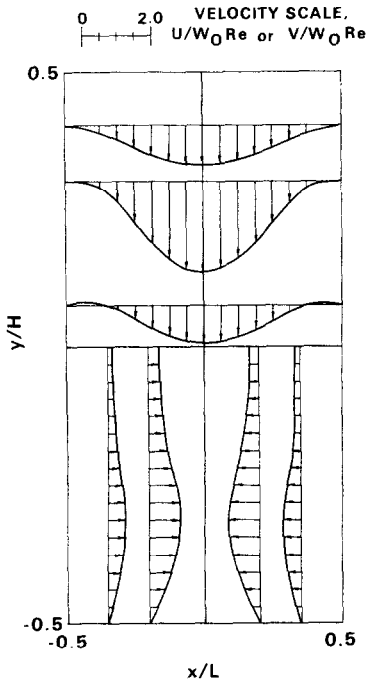

FIG. 8. Secondary flow velocity profiles for a duct with 2:1 aspect ratio, $(z/D)/\mathrm{Re} = 0.0158$.

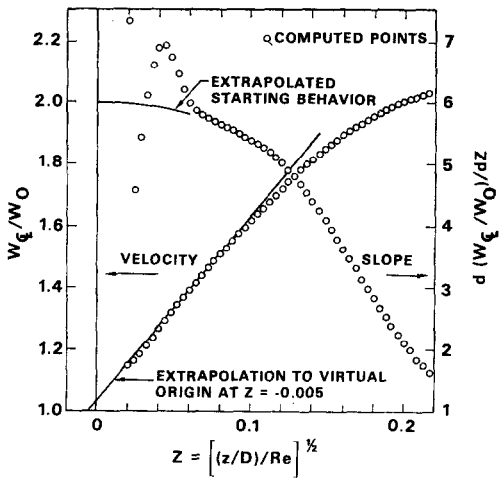

FIG. 9. Determination of virtual origin in the square duct solution: centerline velocity ratio, w_{CL}/w_0, and its slope, $d(w_{CL}/w_0)/dZ$ vs nondimensional axial variable $Z = [(z/D)/\mathrm{Re}]^{1/2}$.

buoyancy force in Eq. (7) was computed using T_w as the reference temperature. The solution was computed for Prandtl number, $Pr = \nu/\alpha = 0.73$; Rayleigh number, $Ra = g\beta(dT_w/dz)\, D^4/\nu\alpha = 103$; and $Re = 1000$. A nondimensional temperature θ, is introduced such that $\theta = (T - T_w)/(dT_w/dz)\, D$. This solution reaches a fully developed condition in which the velocity field and nondimensional temperature do not vary with axial distance. Selected secondary-flow velocity profiles for the fully developed region of this solution are given in Fig. 10. The secondary flow consists of a pair of axial or streamwise vortices driven by thermal convection. The fully developed axial velocity and temperature profiles in the $y = 0$ plane are shown in Fig. 11, and these are found to be in excellent agreement with a solution computed by Cheng and Hwang [15] using a relaxation procedure which is applicable to the fully developed flow regime. This comparison provides one test of the present method for a case with relatively strong interaction between primary and secondary flows. Although results are given here only for the fully developed flow region, the solutions were well behaved in the developing region. The product $RaRe = 1.03 \times 10^5$ is the highest considered in [15]. Although the present numerical method remained stable for a solution with $RaRe = 1.03 \times 10^6$, higher values of RaRe would require special provisions for mesh refinement near the walls and were not attempted.

In each of the present solutions, advantage was taken of the symmetry of the

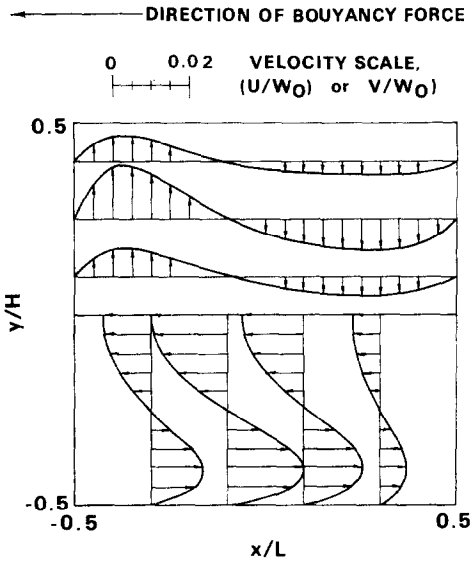

FIG. 10. Fully developed secondary flow velocity profiles for the mixed convection problem in a square duct: Pr = 0.73, Re = 1000, Ra = 103.

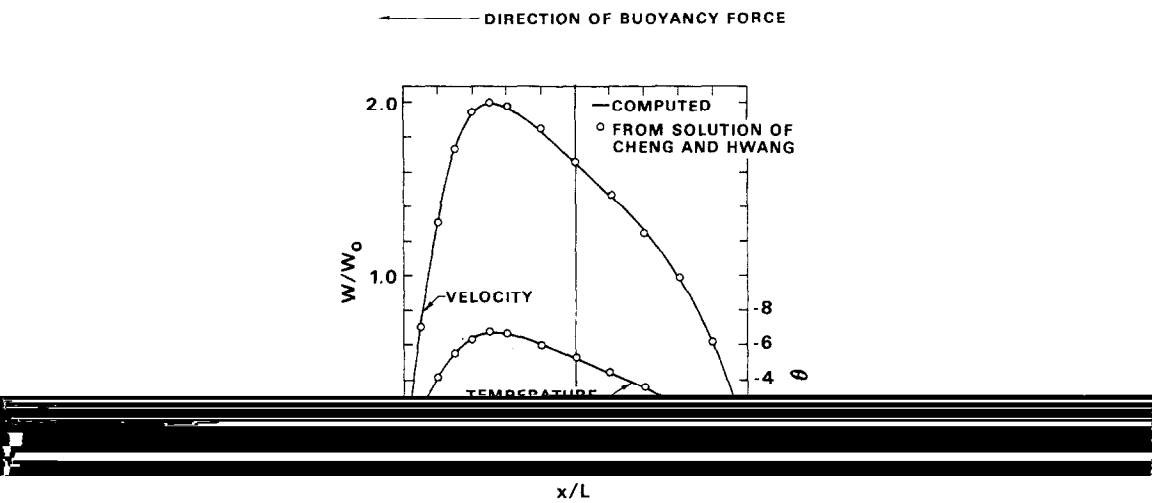

FIG. 11. Fully developed nondimensional axial velocity w/w_0, and temperature θ, profiles for the mixed convection problem in a square duct: Pr = 0.73, Re = 1000, Ra = 103, $y/H = 0$.

flow field about the $y = 0$ plane by a straightforward modification of boundary conditions. The solutions were computed using 21 × 11 and 21 × 21 grids for the 1:1 and 2:1 ducts, respectively, required about 75 axial steps to reach the fully developed region, and required 2 to 5 minutes of UNIVAC 1108 computer time.

ACKNOWLEDGMENT

This work was sponsored as a part of the United Aircraft Research Laboratories Corporate-sponsored program.

REFERENCES

1. W. R. HAWTHORNE, The applicability of secondary flow analysis to the solution of internal flow problems, in "Fluid mechanics of internal flow" (Gino Sovran, Ed.), pp. 238–265, Elsevier, New York, 1967.
2. H. B. SQUIRE AND K. G. WINTER, *J. Aeron. Sci.* **18** (1951), 271.
3. M. ROWE, *J. Fluid Mech.* **43** (1970), 771.
4. A. R. STUART AND R. HETHERINGTON, The solution of the three variable duct flow equations, presented at the 1970 conference on fluid mechanics of turbomachinery, Pennsylvania state university.
5. S. V. PATANKAR AND D. B. SPALDING, *Internat. J. Heat Mass Transfer* **15** (1972), 1787.
6. L. S. CARETTO, R. M. CURR, AND D. B. SPALDING, *Comput. Meth. Appl. Mech. and Engr.* **1** (1973), 39.

7. J. DOUGLAS AND J. E. GUNN, *Numer. Math.* **6** (1964), 428.
8. A. RALSTON, "A First Course in Numerical Analysis," p. 323, McGraw–Hill, New York, 1965.
9. G. F. D. DUFF AND D. NAYLOR, "Differential Equations of Applied Mathematics," p. 139, Wiley, New York, 1966.
10. C. E. PEARSON, *Math. Comp.* **19** (1965), 570.
11. R. J. GOLDSTEIN AND D. K. KREID, *J. Appl. Mech.* **34** (1967), 813.
12. E. M. SPARROW, C. W. HIXON, AND G. SHAVIT, *J. Basic Engr.* **89** (1967), 116.
13. G. S. BEAVERS, E. M. SPARROW, AND R. A. MAGNUSON, *Internat. J. Heat and Mass Transfer* **13** (1970), 689.
14. H. S. SCHLICHTING, "Boundary Layer Theory," 4th edit., pp. 168–171, McGraw–Hill, New York, 1960.
15. K. C. CHENG AND G. HWANG, *J. Heat Transfer* **91** (1969), 59.